

Exciton fine-structure splitting of telecom wavelength single quantum dots: statistics and external strain tuning

Luca Sapienza,^{1,*} Ralph N. E. Malein,¹ Christopher E. Kuklewicz,¹
 Peter E. Kremer,¹ Kartik Srinivasan,² Andrew Griffiths,³ Edmund
 Clarke,³ Richard J. Warburton,⁴ and Brian D. Gerardot^{1,†}

¹*Institute of Photonics and Quantum Sciences, SUPA,
 Heriot-Watt University, Edinburgh, United Kingdom*

²*Center for Nanoscale Science and Technology,
 National Institute of Standards and Technology, Gaithersburg, MD 20899, U.S.A.*

³*EPSRC National Centre for III-V Technologies,
 University of Sheffield, United Kingdom*

⁴*Department of Physics, University of Basel,
 Klingelbergstrasse 82, CH-4056 Basel, Switzerland*

(Dated: March 6, 2013)

Abstract

In a charge tunable device, we investigate the fine structure splitting of neutral excitons in single long-wavelength InGaAs quantum dots as a function of external uniaxial strain. Nominal fine structure splittings between 22 and 106 μeV are measured and manipulated. We observe varied response of the splitting to the external strain, including positive and negative tuning slopes, different tuning ranges, and linear and parabolic dependences. This behaviour is due to a unique critical stress required to achieve the minimum splitting for each quantum dot. These results are promising for the generation of on-demand entangled photon pairs at telecom wavelengths.

*Electronic address: l.sapienza@hw.ac.uk

†Electronic address: b.d.gerardot@hw.ac.uk

Remarkable progress in the field of self-assembled quantum dots (QDs) has been made in the last decade, primarily using InGaAs QDs emitting at $\lambda < 1 \mu\text{m}$ due to the availability of high-efficiency photon detectors. One such noteworthy result is the demonstration of on-demand polarisation entangled photons from a single QD via the biexciton-to-exciton-to-vacuum state cascade [1–3]. However, single-photon sources at telecom wavelengths [4–10] are required for efficient communication via fiber, free-space through the atmosphere, or for integration with Silicon photonics. Unfortunately, due to traditional difficulties in photon detection at telecom wavelengths, to date relatively little progress has been made with QDs in the telecom O-band ($\lambda \sim 1310 \text{ nm}$) or C-band ($\lambda \sim 1550 \text{ nm}$) compared to shorter wavelength ($\lambda < 1 \mu\text{m}$) QDs. Different approaches have been used in order to overcome the challenge of telecom photon detection. For instance, photonic crystal cavities [6] or fiber taper waveguides [7] have been used to enhance the spontaneous emission rate and channel the emitted light into a specific optical mode. Frequency up-conversion from telecom to visible wavelength has also been implemented [11] and single-photon superconducting detectors are being developed to achieve a more efficient detection at telecom wavelengths [12].

In typical self-assembled QDs, the rotational symmetry is broken and the electron-hole exchange interaction mixes the bright exciton states into a non-degenerate doublet referred to as a fine-structure splitting (FSS). The FSS doublet is orthogonally polarized in the linear basis and leads to distinguishability in the biexciton-to-exciton-to-vacuum cascade. The magnitude of the FSS is determined by anisotropy in the strain, shape and composition of the dot, as well as from the crystal inversion asymmetry [13, 14]. If the FSS is smaller than the linewidth, the biexciton-to-exciton-to-vacuum cascade can lead to the emission of polarisation-entangled photon-pairs [1–3]. FSS of the order of a few tens of μeV have recently been manipulated and/or cancelled in QDs emitting at $\lambda < 1\mu\text{m}$ via an electric field [1, 15, 16], uniaxial strain [17–19] or combined electric field and strain [20].

Here we characterise the FSS in long-wavelength QDs and investigate the prospect of minimizing it using uniaxial strain. We investigate two samples containing QDs emitting photons near the telecom O-band: one sample consists of QDs in the bulk and the other is a charge tunable QD device [21]. In the second sample, deterministic charging allows clear identification of the charged excitonic states visible in the photoluminescence (PL) spectra which allows us to selectively address single exciton and biexciton lines. By carrying out

polarisation-resolved PL we measure FSS as low as a few tens of μeV . By applying uniaxial strain [17–20], we demonstrate manipulation of the FSS and reveal different critical stresses (defined as the stress required to reach the minimal FSS) and minimal FSS for different QDs. The incorporation of a second tuning knob [20], e.g. electric fields [1, 15, 16, 20] or another strain axis [22], would make this system a promising candidate for a source of polarisation entangled photons at telecom wavelengths.

The samples consist of a single layer of self-assembled InAs QDs in an $\text{In}_{0.18}\text{Ga}_{0.82}\text{As}$ quantum well (dot-in-a-well, or DWELL structures). Such a structure red-shifts the emission wavelength of the QDs to a wavelength range between 1080 and 1310 nm at $T = 4$ K [7, 8, 10]. As these QDs have deeper confinement potentials than QDs at $\lambda < 1 \mu\text{m}$, a reduced tunnel barrier thickness (14 nm) is required to obtain sharp charge state transitions in PL characterisation as a function of applied bias in the charge tunable device (see Fig. 1a) [23]. The structure, shown in Fig. 1a, has a relatively large (104 nm) capping layer separating the QD and the AlGaAs superlattice to minimize the effect of localised defects at the AlGaAs interface [24]. This device geometry gives a lever arm, defined as the ratio between the device length (400 nm) and the tunnel barrier thickness (15 nm), of ~ 27 which results in an operating voltage of ~ -7.5 V for charging the QD ground state. We optically excite the single QDs by using a non-resonant continuous-wave laser ($\lambda = 830$ nm) and collect the emitted photons with confocal micro-PL. A ZrO_3 super-solid immersion lens (SIL) is positioned on the surface of the sample to increase the collection efficiency and reduce the excitation and collection spot size [25]. With the super SIL, we obtain saturation counts up to ~ 300 Hz on a liquid-Nitrogen cooled InGaAs detector array (equivalent to a photon count rate of $\sim 2 \times 10^4$ Hz). Our spectrometer has a resolution of 0.10 nm ($75 \mu\text{eV}$) at 1300 nm and, using a double Lorentzian fit to the emission lines, we are able to resolve the FSS with a few μeV resolution. The samples under study have a high QD density and spectrally isolated QDs can be found at the tails of the size distribution (between ~ 1080 -1130 and ~ 1240 -1310 nm at $T = 4$ K). To apply the uniaxial strain (along the [110] crystallographic axis), we glue the sample to a piezoelectric lead zirconia titanate (PZT) ceramic stack to which a bias (V_{PZT}) from -300 to +300 V can be applied. These voltages correspond to an upper bound for the applied strain of $\sim \pm 13.9$ MPa (for details on the strain calibration, see [19]).

An example of the PL spectra as a function of the voltage applied to the sample (V_{gate})

is shown in Fig. 1b. Discrete jumps of the emission lines are clearly visible, a signature of Coulomb blockade [21]. To unambiguously identify the neutral exciton (X^0), biexciton ($2X^0$) and single negatively charged exciton (X^{1-}) emission lines, we perform polarisation dependent analysis of the emitted light. An example of the spectra for orthogonal polarisations are shown in Fig. 2b: the emission lines at ~ 1285.3 and ~ 1286.5 nm show FSS, while the line at ~ 1288.9 nm does not shift with changing polarisation. In Fig. 2c, we show the polarisation dependence of the two neighboring emission lines: for orthogonal polarisations one peak shifts towards shorter and one towards longer wavelengths as expected for X^0 ($\lambda \sim 1285.3$ nm) and $2X^0$ ($\lambda \sim 1286.5$ nm), see inset of Fig. 2a. Due to the Coulomb blockade signature (see Fig. 1b) and the absence of any FSS, the emission line at ~ 1288.9 nm is attributed to the X^{1-} recombination from the same QD.

The FSS is measured for several single QDs. Combining the statistics from both samples, we see a full range of FSS between 22 and 106 μeV for 51 measured QDs (Fig. 2a). This range of FSS is considerably smaller than previous reports on FSS for QDs emitting at similar wavelengths [5, 10, 26], an important result as a smaller initial FSS requires more modest external fields for complete cancellation.

We next apply an external uniaxial strain and find that the FSS can be manipulated in a reversible way and that significant reductions of the FSS can be achieved (see Fig. 3). Table I summarizes the results from 12 single QDs. We observe tuning ranges (Δ FSS) from 8.3 to 46.4 μeV , slopes ranging from -0.015 to 0.077 $\mu\text{eV}/V_{PZT}$, and blueshifts of the emission energy ΔE of ~ 1 meV for increasing tensile strain. In Fig. 3a, we show a polar plot for the two orthogonally polarized exciton lines for QD10. As shown, going from -300 to +300 V_{PZT} , the alignment of the polarisation angle θ with respect to the [110] axis only varies by a few degrees, a typical result in our experiments. While most of the QDs under study show a linear dependence of the FSS as a function of the applied strain (see Fig. 3b left panel), for QD2 we observe a parabolic modification of the FSS which reaches a minimum of 22.4 ± 2.2 μeV (see Fig. 3b right panel).

The application of uniaxial strain is expected to modify the FSS in a quadratic way, with the minimum of the parabola representing the minimal FSS that is reachable for a specific QD [1, 20]. The critical stress required to reach the minimum FSS depends on the shape and composition of each specific QD [13, 14]. If the critical stress is not experimentally reachable, one observes only linear reductions with either positive or negative tuning slopes,

TABLE I: Strain tuning of single QDs. The wavelength λ is the central wavelength of the excitonic line without applied external strain. The FSS slope is the result of a linear fit of the FSS splitting in the full V_{PZT} range, except for QDs 2, 9, 12 where only the points in the linear regime were fitted (see Fig. 3c). The angle θ represents the polarisation angle of the low energy peak with respect to the [110] crystallographic axis. FSS_{min} is the minimal value of FSS that we measure in our experiments. ΔE refers to the energy shift for the full tuning range for increasing tensile strain.

QD	$\lambda_{V_{PZT}=0}$ (nm)	$FSS_{V_{PZT}=0}$ (μeV)	FSS slope ($\mu\text{eV}/V_{PZT}$)	Δ FSS (μeV)	FSS_{min} (μeV)	ΔE (meV)	$\theta_{V_{PZT}=0}$ ($^\circ$)
1	1167.0	45.2 \pm 2.1	0.015	8.3	35.7	0.91	83.6
2	1224.7	23.5 \pm 2.4	-0.074	15.1	20.1	0.99	-5.9
3	1227.3	41.0 \pm 3.4	-0.036	21.8	23.1	0.82	-2.9
4	1228.0	46.0 \pm 5.9	-0.022	12.4	37.5	0.82	-2.9
5	1234.0	39.5 \pm 1.1	0.026	15.6	28.9	0.81	-0.1
6	1234.4	34.4 \pm 0.9	0.024	13.0	29.3	0.81	0.8
7	1235.3	32.2 \pm 0.7	0.022	13.8	21.5	0.81	-1.5
8	1241.2	47.2 \pm 2.1	0.077	46.4	22.5	0.72	0.7
9	1267.0	49.7 \pm 5.1	0.051	19.9	49.0	0.70	1.3
10	1285.7	50.3 \pm 2.6	-0.021	14.2	47.3	0.75	92.8
11	1288.0	47.2 \pm 1.2	-0.017	10.3	39.1	0.90	-8.6
12	1296.2	68.6 \pm 2.5	-0.024	11.1	63.3	0.74	-9.9

depending on which arm of the parabola is probed (see Fig. 3b). The application of larger strain would enable the minimum of the parabola to be reached for each dot and a second external field would possibly allow complete cancellation of the FSS.

QDs with exciton polarisation aligned along the [110] or [100] directions are expected to reach the smallest FSS when an external stress is applied [14]. As shown in Table I, we find that most of the QDs are aligned with the [110] axis. No post selection has been done to the data to select QDs better aligned to the crystallographic axis, suggesting that the QDs are primarily aligned along the same axis, in contrast to shorter wavelength (~ 950 nm) smaller

QDs whose alignment is more random [27]. The small rotations of the polarisation angle shown in Fig. 3a are expected when the FSS varies linearly with the applied strain. We also note that for QD2 the rotation of the polarisation angle is still limited to $\sim 5^\circ$, even though we are able to reach the minimal FSS. Polarisation rotations smaller than the ones reported in References [1] and [20] have been predicted for QDs with different shapes and composition [13, 14]. Further investigation is required to correlate the shape and composition with the polarisation angle rotation in these QDs.

In conclusion, we have realised a charge tunable structure for QDs emitting at telecom wavelengths to enable deterministic charging of the neutral exciton. By performing polarisation-resolved PL, we observe nominal FSS of neutral exciton lines down to $22 \mu\text{eV}$. We demonstrate that the application of uniaxial strain allows significant manipulation of the FSS and we observe linear reductions of the FSS for most of the QDs. Each QD shows a unique response to the applied strain, which is attributed to different structural properties of the QDs that result in different values of critical stress required to reach the minimal FSS. These results are a promising step in bridging the gap in the state-of-the-art between mature QDs emitting at $\lambda < 1\mu\text{m}$ and telecom wavelength QDs.

The authors would like to thank A. Dada for comments on the manuscript and acknowledge the financial support for this work from the Royal Society, EPSRC, and NCCR QSIT.

-
- [1] A. J. Bennett et al., Nat. Phys. **6**, 947 (2010).
 - [2] A. Dousse et al., Nature **466**, 217 (2010).
 - [3] N. Akopian et al., Phys. Rev. Lett. **96**, 103501, (2006).
 - [4] M. B. Ward et al., Appl. Phys. Lett. **86**, 201111 (2005).
 - [5] M. B. Ward et al., J. Phys.: Conf. Ser. **210**, 012036 (2010).
 - [6] L. Balet et al., Appl. Phys. Lett. **91**, 123115 (2007).
 - [7] K. Srinivasan et al., Appl. Phys. Lett. **91**, 091102 (2007).
 - [8] B. Alloing et al., Appl. Phys. Lett. **86**, 101908 (2005).
 - [9] N. A. J. M. Kleemans et al., Phys. Rev. B **79**, 045311 (2009).
 - [10] A. I. Tartakovskii et al., Appl. Phys. Lett. **88**, 131115 (2006).
 - [11] M. T. Rakher et al., Nat. Phot. **4**, 786 (2010).

- [12] M. G. Tanner et al., Appl. Phys. Lett. **96**, 221109 (2010).
- [13] R. Singh and G. Bester, Phys. Rev. Lett. **104**, 196803 (2010).
- [14] M. Gong et al., Phys. Rev. Lett. **106**, 227401 (2011).
- [15] B. D. Gerardot et al., Appl. Phys. Lett. **90**, 041101 (2007).
- [16] K. Kowalik et al., Appl. Phys. Lett. **91**, 183104 (2007).
- [17] S. Seidl et al., Appl. Phys. Lett. **88**, 203113 (2006).
- [18] J. D. Plumhof et al., Phys. Rev. B **83**, 121302R (2011).
- [19] C. E. Kuklewicz et al., Nano Lett. **12**, 3761 (2012).
- [20] R. Trotta et al., Phys. Rev. Lett. **109**, 147401 (2012).
- [21] R. J. Warburton et al. Nature **405**, 926 (2000).
- [22] J. Wang et al. Appl. Phys. Lett. **101**, 063114 (2012).
- [23] M. Ediger et al., Nature Physics **3**, 774 (2007).
- [24] J. Houel et al., Phys. Rev. Lett. **108**, 107401 (2012).
- [25] K. A. Serrels et al., Journal of Nanophotonics **2**, 021854 (2008).
- [26] N. I. Cade et al., Phys. Rev. B **73**, 115322 (2006).
- [27] S. Seidl et al., Physica E **40** 2153 (2008).

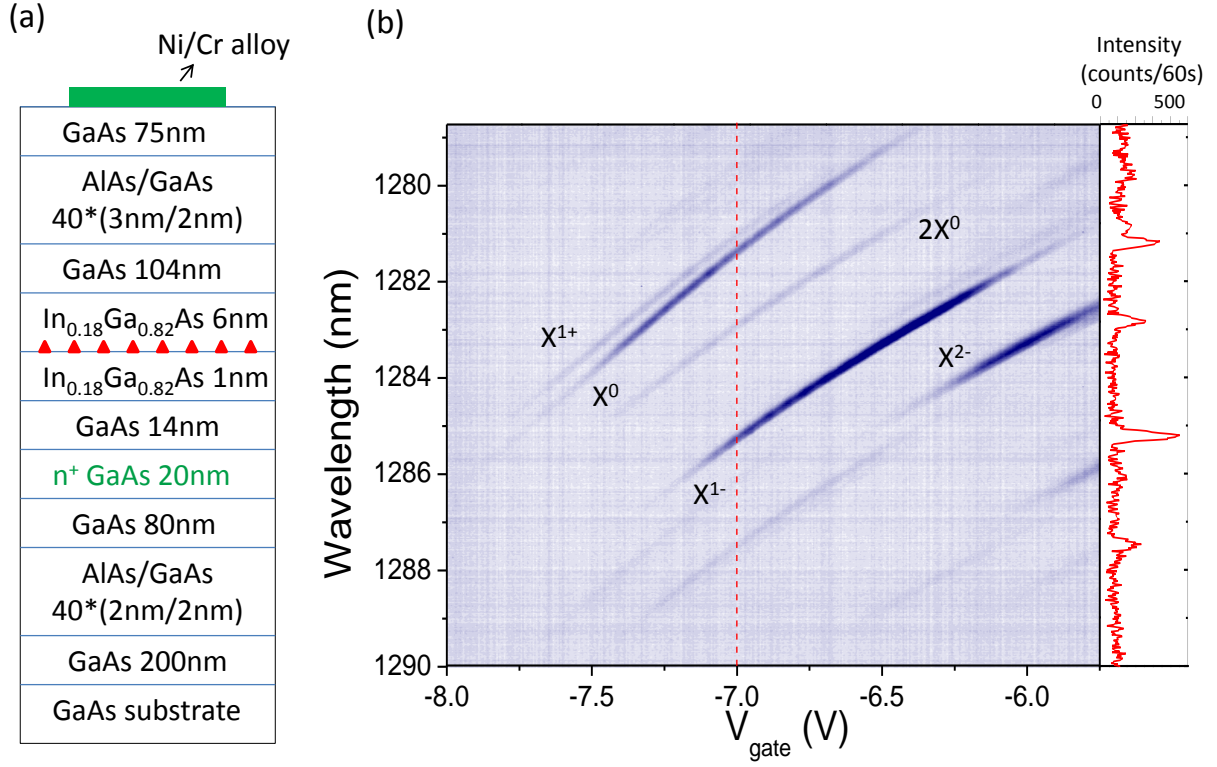


FIG. 1: (a) Schematic of the charge tunable structure. The red triangles represent the QD layer. (b) PL spectra collected as a function of the applied gate voltage under non-resonant excitation ($\lambda = 830$ nm) at a temperature $T = 4$ K. The peaks corresponding to the emission from different states of a single QD are labeled accordingly. The right panel shows a linecut of the contour plot at the corresponding red dashed line, at $V_{gate} = 7$ V.

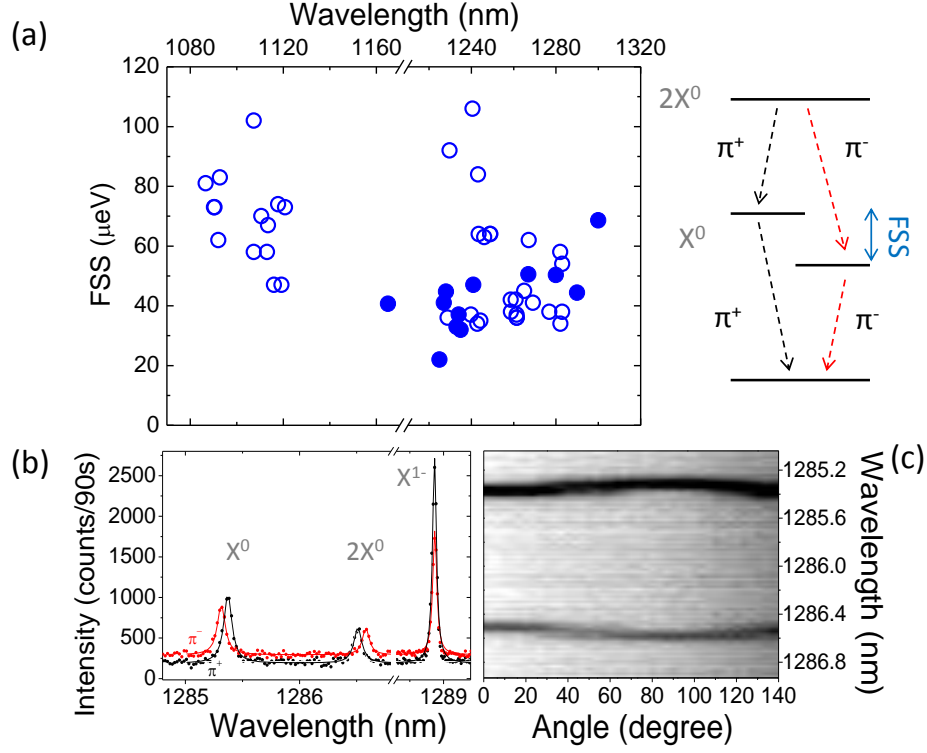


FIG. 2: (a) FSS measured on single QDs. The full symbols represent values obtained from the charge tunable device, while the open symbols correspond to measurements from a layer of DWELL QDs grown in the bulk. The inset represents a schematic of the biexciton ($2X^0$)-to-exciton (X^0)-to-vacuum state transitions and their respective polarisations (π^+ or π^-). (b) An example of PL spectra at orthogonal polarisations, showing the X^0 , $2X^0$ and singly charged exciton (X^{1-}) emission lines (full symbols) and a Lorentzian fit to the data (solid lines). The two data sets are extracted from the polarisation scan shown in panel c (at an angle of 0 and 90°). (c) Contour plot of the X^0 and $2X^0$ polarisation-resolved PL spectra.

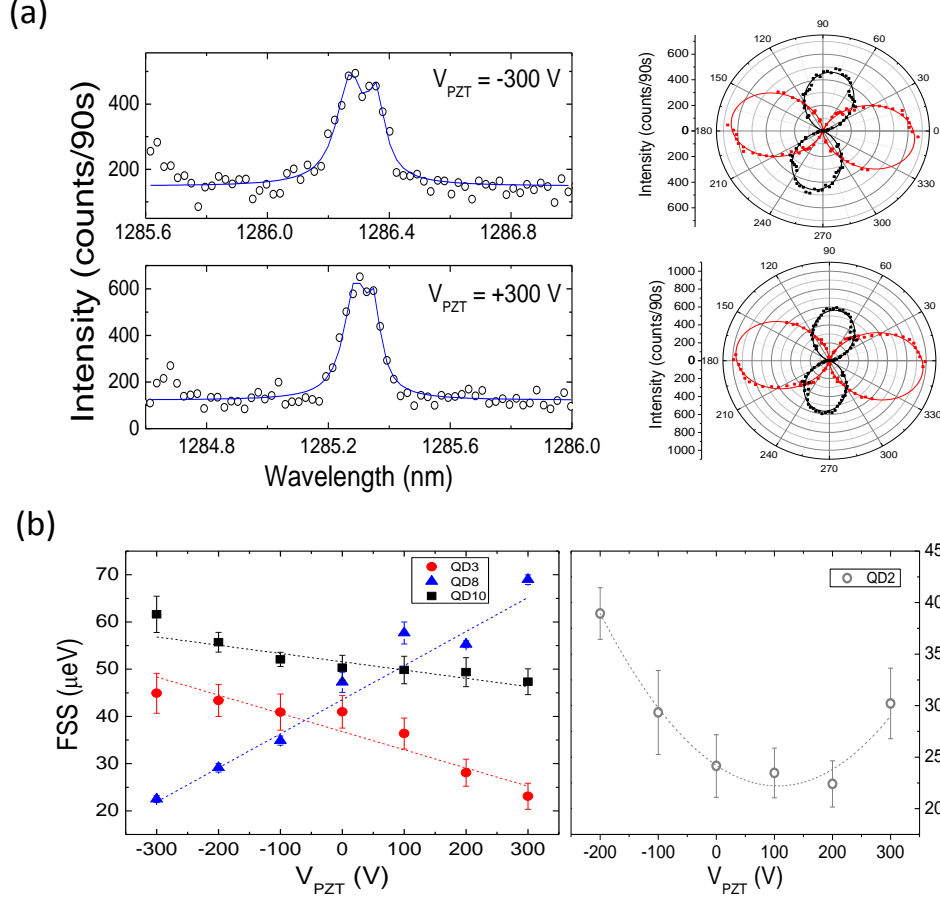


FIG. 3: (a) Left panel: Example results of the manipulation of the X^0 FSS of QD10 with uniaxial strain. The solid lines are double Lorentzian fits to the data, collected at a polarisation angle of $\sim 45^\circ$ (open circles). Right panel: Two examples of polar plots for the two orthogonal exciton lines at $V_{PZT} = -300, +300$ V. The solid lines are fits to the data. (b) FSS as a function of applied voltage on the PZT stack for four different single QDs. The error bars are the standard deviation from the mean value of the FSS, obtained from 43 fits to the experimental spectra collected as a function of polarisation angle ranging between 0° and 140° . The dashed lines in the left (right) panel are linear (quadratic) fits to the data.